Molecular dynamics studies of the dissociated screw dislocation in silicon

2010 J. Phys.: Condens. Matter 22 074210

(http://iopscience.iop.org/0953-8984/22/7/074210)

IOP Publishing Journal of Physics: Condensed Matter

J. Phys.: Condens. Matter **22** (2010) 074210 (8pp) doi:10.1088/0953-8984/22/7/074210

Molecular dynamics studies of the dissociated screw dislocation in silicon

R Choudhury[1], C Gattinoni[1], G Makov[1,2] and A De Vita[1]

[1] Physics Department, King's College London, Strand, London WC2R 2LS, UK
[2] Department of Materials Engineering, Ben Gurion University of the Negev, Beer-Sheva 84105, Israel

Received 24 September 2009, in final form 17 November 2009
Published 3 February 2010
Online at stacks.iop.org/JPhysCM/22/074210

Abstract

Characterizing the motion of dislocations through covalent, high Peierls barrier materials is a key problem in materials science, while despite the progress in experimental studies the actual observation of the atomistic behaviour involved in core migration remains limited. We have applied a hybrid embedding scheme to investigate the dissociated screw dislocation in silicon, consisting of two 30° partials separated by a stacking fault ribbon, under the influence of a constant external strain. Our 'learn on the fly' hybrid technique allows us to calculate the forces on atoms in the vicinity of the core region using the tight binding Kwon potential, whilst the remainder of the bulk matrix is treated within a classical approximation. Applying a 5% strain to the dissociated screw dislocation, for a simulation time of 100 ps at a temperature of 600 K, we observe movement of the partials through two different mechanisms: double kink formation and square ring diffusion at the core. Our results suggest that in these conditions, the role of solitons or anti-phase defects in seeding kink formation and subsequent migration is an important one, which should be taken into account in future studies.

1. Introduction

Dislocations play a key role in the deformation of materials as the carriers of plasticity, allowing materials to yield at stresses far lower than those required to deform the perfect bulk crystal. Given their importance, developing our understanding of the atomic scale processes involved in dislocation migration remains a key challenge in materials science. Though classical elasticity theory based approaches have yielded great insight into the interaction of such defects with their surrounding crystal environment [1], the analytic expressions become singular when extrapolated into the dislocation core regions, and are thus unsuitable to understand the atomistic behaviour of the core, for example in response to the application of an external force.

Semiconductor device heterostructures and thin film devices are increasingly important technologically. The presence of dislocations in semiconductors can lead to degradation of their electronic properties, since such defects can alter the density, mobility and lifetime of electrical carriers, as well as to mechanical failure. Semiconductors are materials with a high Peierls barrier, as the covalent bonds lead to a brittle lattice structure. As such, sub-Peierls dislocation motion is expected to occur through the formation and subsequent migration of kinks along the dislocation line [1]. The energetic cost of kink formation leads to low dislocation velocities relative to other materials, such as metals, which have comparatively low barriers to dislocation motion.

In silicon much experimental work has been performed to characterize the structure and behaviour of the different occurring dislocation types. As silicon is the simplest high Peierls barrier semiconductor, it forms an excellent prototype for the study of dislocations in this class of materials. The experimental work of Ray and Cockayne [2] established that dislocations in silicon are dissociated, motivating the study of the 30° and 90° partials rather than the 60° and the perfect screw dislocations. The partials are separated by an intrinsic stacking fault [3, 4], and lie on {111} type close-packed glide planes. The experimental consensus is that they are electrically inactive in their reconstructed forms [5–7], and that any electrical activity should be associated with impurities or defects located along the dislocation line.

Complementing the experimental work on silicon are many computational studies [8–13], which have focused on obtaining kink formation and migration energies from static calculations, since meaningful molecular dynamics simulations have, until now, been too expensive to perform on systems which must contain, at the minimum, tens of

thousands of atoms. Kinetic Monte Carlo simulations [14, 15] have also been performed, taking the kink energies as parameters from atomistic calculations in order to extrapolate system behaviours up to the mesoscale. For a good review of both the experimental and computational situation one may turn to [16].

Of the partial pair, the 30° partial is the mobility-controlling dislocation in silicon, as it has a lower velocity than the 90° partial. The kink energies of the 30° partial have been estimated using both DFT [8] and tight binding (TB) [12]. This dislocation has also been studied using the Stillinger–Weber (SW) classical potential [13], which is able to reproduce the correct reconstructed ground state in which dimers lie along the dislocation line. In [12] soliton defects (undimerized undercoordinated Si atoms) along the dislocation line are also examined within the TB approximation, and these same defects have also been studied using *ab initio* techniques in [17]. Reference [17] established that the soliton is the fundamental excitation of the reconstructed core, and thus plays an important role in the plastic flow of the material. In fact, the effect of impurities and reconstruction defects on dislocation motion, although not a part of the classic Hirth and Lothe [1] picture, is likely to be very significant [18]. Previous studies find a low energy barrier to the migration of what are called solitons or phase switching defects along the dislocation line, a behaviour we are able to monitor in the simulations as discussed in section 3.2, during which we observe these defects at high temperature and strain. To our knowledge, no previous electronic structure based dynamical simulations of kink formation and migration in the 30° partial have been carried out to date, due to the computational expense of simulating a system containing many thousands of atoms for the order of hundreds of picoseconds, which is the length of the simulation time necessary to observe the core migrate through several Peierls valleys. In order to make a dynamical simulation tractable, in the present work we employ the 'learn on the fly' (LOTF) hybrid embedding scheme [19]. The LOTF method has had much success in the description of crack propagation, capturing features of the tip reconstruction and mobility [20], and has also been successfully applied to hydrogen platelets in silicon [21]. In section 2, we provide details of the application of the scheme to the problem of accurately representing the stress tensor field associated with the presence of partial dislocations in a Si matrix and simulating dislocation motion. The success of LOTF in applications involving silicon is in no small part due to the availability of an excellent classical potential, due to Stillinger and Weber [22], to describe the bulk matrix making up the greater part of our hybrid simulation cells. For the problem of interest here, this potential is used to ensure the effective propagation of an applied external strain to the localized, chemically active dislocation cores, which are treated within the tight binding approximation [23].

2. Methodology

The LOTF hybrid scheme combines the computational efficiency of classical potentials with the precision of quantum mechanical (QM) methods thus allowing the study of problems requiring big systems (∼100 000 atoms) as well as ensuring high accuracy, whenever required, in specific areas of the system [19]. The forces used in the scheme are derived from a universal potential whose parameters are vary in time and across the system, being tuned 'on the fly' during the simulation [26]. The aim of the tuning (parameter optimization) procedure is to reproduce the correct target forces which are, in our case, the SW force for the atoms in the classical zone and the forces obtained from the Kwon TB model Hamiltonian in the quantum zone. A buffer region between the QM and classical zone is used to ensure a smooth transition between the two potentials [27] and to handle moving boundary regions accurately [20] while still enforcing momentum conservation.

The atom-resolved values of the stress tensor associated with the LOTF relaxed geometries are obtained from the local values of the strain tensor, by applying the linear theory of elasticity. A definition of the atom-resolved stress tensor is obtained for all the four-fold coordinated Si atoms in the system (all other atoms are assigned zero stress). Namely, we compare the relative atomic positions with those of a reference unstrained Si crystal, once rotations are factored out by a straightforward matrix decomposition method, to compute the strain tensor components and, from these, the stress components via the elastic constants. As a first application of our toolset, we compare the stress components obtained by the purely SW and hybrid LOTF schemes with the results predicted by classical elasticity theory in a representative dislocation geometry.

In figure 1 the LOTF calculated σ_{yy} stress component of a 90° partial dislocation is represented for a range of distances from the dislocation core (solid black line). A second plot shows the results obtained for the same system when the atomic positions are fully relaxed using the SW classical model only for the whole system (broken line). Significant discrepancies between the predictions of the two atomistic models can be seen well beyond the QM/MM boundary distance from the core used in the LOTF method (of the order of a few bond lengths, see inset in figure 2). We take this as an indication that the coupling between the QM and classical zones in the LOTF hybrid system has a crucial effect on the correct representation of the local stress field around the dislocation which the classical potential cannot represent. Given that the local stress field is the primary cause of plasticity behaviour by dislocation migration, this in turn suggests that the latter cannot be expected to be well described in the absence of a proper QM treatment of the inner core region, as we indeed find below. We note that the stress values predicted for a 90° partial dislocation by standard elastic theory [1] are of no use in the proximity of the dislocation core, because of the inverse square root divergence of the classical formulation.

In order to further illustrate the importance of QM force calculations around the dislocation core, we consider the system in figure 2 as a second example, and we calculate the vectors $\mathbf{F}_{(i,j,k)}$ which represent the forces per unit surface area which the stress tensor produces when resolved on specific (i, j, k) planes. The system is a silicon slab with

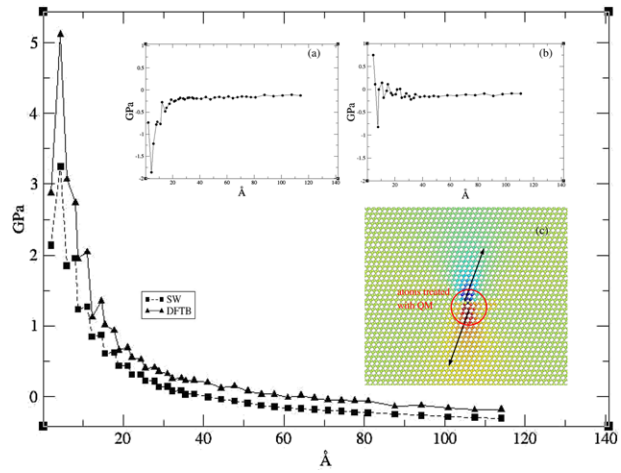

Figure 1. The main graph shows the σ_{yy} component of the stress tensor calculated on a ∼10 nm long line of Si atoms starting from the dislocation core. This extends into the (red-yellow) tensile region of the stress field, in the direction shown by the bottom arrow in inset (c). The dislocation core has been relaxed using the SW potential (broken line) and the LOTF scheme (solid line). The difference between the two plots is shown in inset (a) on a magnified scale, showing that SW produces significantly less core deformation for the same external load. A similar analysis carried out for the compressive (blue) zone (upper arrow direction in inset (c)) produced the stress difference shown in inset (b), showing much smaller deviations.

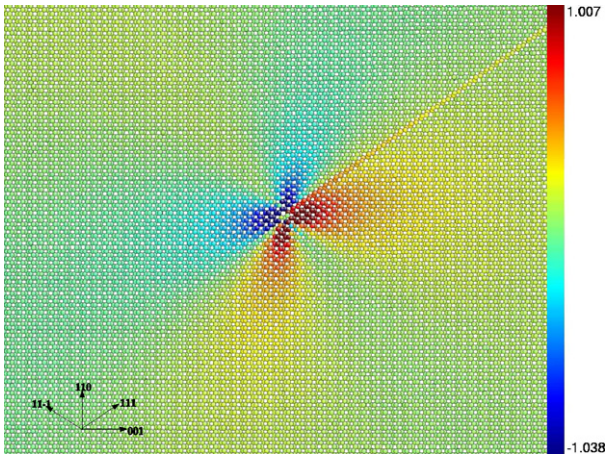

Figure 2. Representation of the force difference $F^{\perp}_{(1,1,1)} - F^{\perp}_{(1,1,-1)}$ in a silicon slab containing a 90° partial dislocation. The colours code allows the identification of the (red-yellow) regions where crack propagation on the (110) cleavage plane in the [001] direction (i.e., horizontally, left to right, in the figure) may deflect to the (111) cleavage planes. In the (blue-green) regions of the plot deflection to $(11\bar{1})$ cleavage planes is expected to be favoured.

the [110] direction aligned vertically, containing a 90° partial dislocation having its core aligned with the $[1\bar{1}0]$ direction perpendicular to the figure plane, and associated with a (111) stacking fault plane. In such a configuration it is not *a priori* clear how the inter-atomic bonds are compressed or stretched in the surroundings of the dislocation core. The quantitative description of these subtle effects is, however, crucial for making predictions on the mechanical properties of the material. This is e.g., the case in problems involving fracture propagation instabilities, where the deflection of the cleavage plane during catastrophic brittle fracture is controlled precisely by such effects. Indeed, static stress fields associated with defects such as dislocations, although relatively weak if compared with the tip-enhanced primary uniaxial tension powering crack propagation, are experimentally known to cause crack deflection [24].

The role of dislocations in generating crack propagation instabilities will be investigated in detail in a forthcoming work [25]. Here we present a preliminary analysis to illustrate to which extent qualitative predictions on the system's mechanical properties may depend on an accurate description of the elastic fields in a dislocation core region. For a Si(110)$[1\bar{1}0]$ crack propagating in the [001] direction (i.e. left to right horizontally in figure 2) instabilities could occur where the crack would deflect onto the (111) planes, even if the external load were purely tensile (i.e. limited to the σ_{yy} component). Such a phenomenon would be actively promoted if the stress field induced by the dislocation (not limited to the σ_{yy} component), produced different effects when resolved on the (111) and $(11\bar{1})$ plane systems. For instance, since the connecting bonds between (111) planes are orthogonal to the planes, the most relevant quantity for bond stretching/breaking is just the [111] component of $\mathbf{F}_{(1,1,1)}$, a scalar field $F^{\perp}_{(1,1,1)}$ which can be readily calculated from the stress tensor. The difference between this and the analogous $F^{\perp}_{(1,1,-1)}$ scalar field is small, everywhere smaller than ∼1 GPa (figure 2). However, it reveals the regions of the system where a deflection to the (111) or $(11\bar{1})$ cleavage planes are favoured, opening the way to fracture path prediction [25] consistent with the observations [24]. Once again, in this example the high accuracy of a scheme including QM models is necessary for capturing the relevant physical effect. Indeed, small stress field asymmetries induced by the dislocation in a much larger, tip-concentrated, symmetric external load are the driving element of the instability and they must be accurately calculated.

We next come to the system geometry we used to simulate dislocation migration. We introduce the 30° partials into bulk {111} oriented silicon by setting the core of each partial at a distance $+/-(d)$ along the $[11\bar{2}]$ direction from the centre of the simulation cell, and then displacing the atoms in the cell in accordance with the classical strain fields [1]. This results in a pair of unreconstructed 30° partials with Burgers vectors which sum to that of a screw dislocation, with a stacking fault (SF) ribbon lying between them. In our simulations the initial distance between the partials (the ribbon length) is set to 34 Å. The choice of the initial distance has implications which we will touch upon in section 3. In the standard theory an energy cost is associated with introducing a SF into the bulk matrix, which is balanced by the repulsive interaction between the dislocations to define an optimal distance between the two partials. We note, however, that in the SW model the SF energy is zero due to the short range of the interaction, so that the energy balance between creation of the SF region against increasing distance between the two partials is not captured by our model.

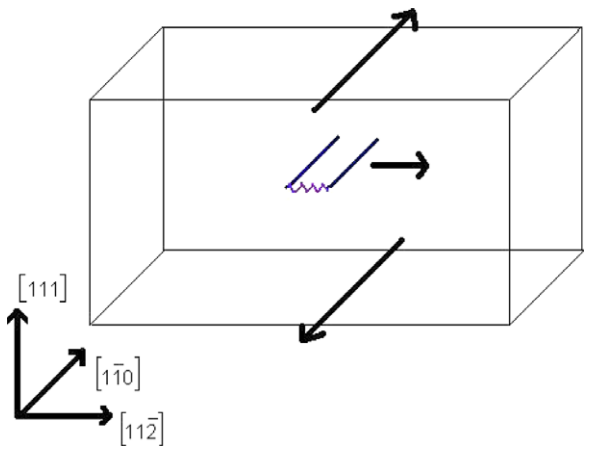

Figure 3. Diagram showing simulation setup; a constant strain is applied in the direction of the black arrows at the top and bottom surfaces of the simulation cell, causing the partials to migrate in the [11$\bar{2}$] direction.

Figure 3 presents a schematic of our simulation. The two cores are shown as blue lines close to the cell centre. The arrows along the top and bottom (111) surfaces illustrate our application of a shear strain across the glide plane in order to induce the partials to migrate in the direction of the shown arrow, [1$\bar{1}$0]. As also shown, the simulation cell unit vectors are $\mathbf{a} = \frac{a_0}{2}[111]$, $\mathbf{b} = \frac{a_0}{2}[1\bar{1}0]$ and $\mathbf{c} = \frac{a_0}{2}[11\bar{2}]$. The cell is periodic along the [1$\bar{1}$0] direction only. The cell dimensions are 261.3 Å along [11$\bar{2}$], 30.96 Å along [1$\bar{1}$0] (the periodic core axis) and 133.75 Å along [111], and there are 41 472 atoms in the simulation cell in total. The lattice is scaled to the SW lattice constant [22] $a_{\mathrm{sw}} = 5.43$ Å.

The core of the 30° partial itself has a double period reconstructed structure [12], due to dimerization occurring along the dislocation line. In order to relax the dislocation cores from their initial unreconstructed configuration we allow the simulation cell to relax for 5 ps at 300 K, without applying any shear strain. Using the LOTF [19, 20] scheme, we apply forces from the Kwon [23] TB potential to the atoms along the core and to atoms within a 4 Å radius (in the directions defined by **a** and **c**). This produces a tubular QM region which follows the dislocation line, with classical SW forces applied to the remainder of the cell.

To induce dislocation motion we must apply a force along the line of the dissociated screw dislocation, which is achieved by applying a constant shear strain to the system as schematically shown in figure 3. Three atomic layers at both the top and bottom of the simulation cell are held fixed for the duration of the simulation, ensuring that a constant strain is present at all times.

In order to evaluate the force on a given atom in the dislocation core, we consider only atoms which are up to three nearest neighbour hops away. The cluster thus selected is then terminated by hydrogen atoms to passivate the spurious surface dangling bonds. The selected cluster is then passed to the Kwon tight binding Hamiltonian 'black box' routine of the LOTF scheme for force evaluation. As we use only a localized cluster of atoms to obtain the QM force, this step of the molecular dynamics algorithm is easily parallelized by sending the cluster for each separate atom in the tight binding region to a different processor, depending on availability (a master–slave approach is used to optimize the computational load balance). Parallelization on 32 standard (Intel Woodcrest) processing elements, allowed us to simulate approximately 10 ps per day, using 1 fs MD time steps. We tested force convergence using cluster sizes from two to six hops, and found that three hops converged forces to within 0.01 eV Å^{-1}.

The Kwon lattice constant is $a_{\mathrm{kw}} = 5.454$ Å, and is thus 0.4% larger than a_{sw}. If neglected, this would give rise to a compressive strain on the dislocation core where forces are calculated using the Kwon TB potential. In order to avoid this effect, we simply rescaled the bond lengths of the atomic clusters which fed into the Kwon tight binding potential, multiplying them by a factor $1 + \epsilon$ where $\epsilon = \frac{a_{\mathrm{kw}}}{a_{\mathrm{sw}}}$. The resulting forces must also then be rescaled by a factor $\frac{1}{(1+\epsilon)}$. The temperature of our simulation cell was set to 600 K, using a Langevin thermostat. This temperature was chosen as a value high enough to expedite kink formation rates, but not so high as to cause melting in the core region, which was only ever observed in test runs at 900 K and above.

Different dislocation core lengths were also considered, ranging from a dimers pair (four lattice periods) up to a twelve dimer core, as the behaviour of the core under strain is dependent on its total length. At one extreme, a core containing only a single dimer is too short to form kinks, and must overcome the Peierls barrier if it is to migrate at all. As we are using periodic boundary conditions along the core direction, any formed kinks will have images in the neighbouring cells, so that interactions with images is an issue for a relatively short repeating core structure. In our work we chose to study the motion of a core of four dimers or eight lattice periods in length. Though this is sufficient for kink formation, there is a possibility of kink-image kink interaction influencing the simulation. However, we cannot perform a size test on core lengths long enough to rule out kink–kink interactions using our classical force model, since as mentioned above, the SW potential does not predict kink formation during dislocation motion. Yet, while simulations using longer cores and different loading modalities are currently ongoing and will be presented in a later paper, we feel that the results discussed below obtained with the present system sizes are sufficient to provide some valuable insight into the behaviour of dislocations in Si. Shear strain can be introduced into the system in a straightforward manner in the simulation cell, by displacing the atoms along the [1$\bar{1}$0] direction as a function of height along [111], according to (1). Here d is the maximum value of the displacement along [1$\bar{1}$0], so that atoms at the top surface of the simulation cell (taking the bottom to be the base [111] surface, i.e. $l_i = 0$) are displaced by d.

$$\delta_{[1\bar{1}0]} = l_i / l_{[111]}(d). \tag{1}$$

3. Results

3.1. Simulations with Stillinger–Weber classical potential

We first explored the system using the SW potential in order to gain an insight into the topological behaviour at a moderate

computational expense. Migration of the partials is observed if a 5% strain is applied to the system by the method described in section 2, and only at 1400 K or above. In these conditions, both lead and trailing partials migrate over 100 Å during a simulation time of about 100 ps. However, these simulations produce only a relatively incoherent core motion, described below, with no obvious connection with kink propagation. In the classic kink propagation mechanism we would expect to see a single double kink nucleated from the straight core of the dislocation and the pair of 'left' and 'right' kinks thus formed travel along the dislocation line, dragging the core into the next lattice position as they do so. Kink formation and migration is a thermally activated process: as such we would expect to see double kink nucleation occurring at an increasing (exponentially dependent) rate on increases in the simulation temperature. Using the Stillinger Weber model we observe no such behaviour, in fact no movement of any kind at all is witnessed within a 100 ps simulation time, at temperatures smaller than ∼1400 K. At ∼1400 K both partials begin their migration into the crystal, by a mechanism which involves local melting of the defect core followed by its recrystallization between one and three lattice steps further away into the crystal, along the propagation motion. To summarize, the SW description of dislocation motion appears incorrect, which is not surprising as a classical three-body potential cannot be expected to accurately reproduce the subtleties of dislocation migration by kink formation and diffusion in silicon. However, the SW model did produce migration of both the lead and trailing partials under an applied strain, as well as an estimate of the simulation time required for motion.

3.2. Simulations with the Kwon tight binding potential

Investigating the migration when forces in the core region were evaluated using the Kwon potential yielded results markedly different from those of section 3.1. We applied once more a 5% shear strain to the 41 472 atom system described in section 2, at a temperature of 600 K maintained using the Langevin thermostat. A 1 fs simulation time step was employed for a total simulation time of 100 ps. In order to locate the core line, it was sufficient to look for one or more dimer pairs (see figure 6) in the glide plane. Test simulations in which the QM region was restricted to the core atoms only, that is to the eight atoms along the dislocation line, showed a behaviour similar to what observed in the simulations using the SW potential, i.e. very little movement even at temperatures close to 1000 K. In particular, no kink formation or migration was ever observed in these simulations. This indicates that the strength of the dimer bond, presumably well reproduced even when using these modestly sized QM zone, is not in itself the limiting factor for kink formation.

Kink formation and dislocation migration was instead obtained once the QM zone was extended to include the first and second nearest neighbours of the core line atoms, i.e. when the Kwon potential was used to evaluate the forces on the atoms lying within a radius of about 7–8 Å from the core line. The position of the lead partial as a function of time during migration is shown in figure 4. Each circled point on the graph

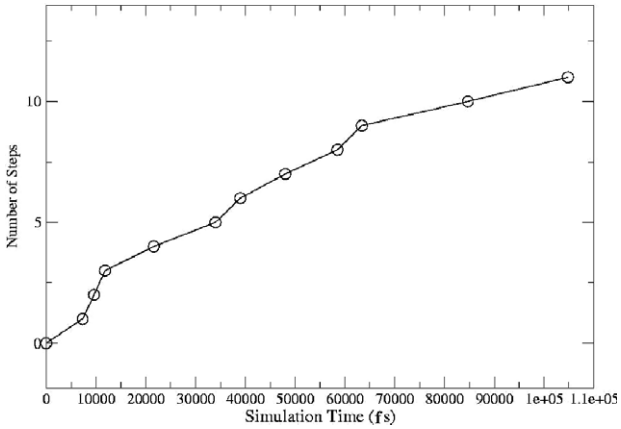

Figure 4. Position of leading partial as a function of time, measured as number of lattice migration steps.

corresponds to a complete migration step into the next Peierls valley, for a total of ten steps occurring over approximately 110 ps. We see a mixture of short and relatively long intervals, consistent with the stochastic nature of kink formation. We note that dislocation migration poses some problems to the definition of the core (QM) region to be used in our hybrid scheme. For instance, during the simulations the dimer bonds at the core temporarily break apart and then reform a few femtoseconds later. Time averaged atomic positions were therefore used to calculate whether atoms were dimerized in the $[1\bar{1}0]$ direction or not, as the temperature and strain result in large atomic oscillations making the instantaneous atomic coordinates unreliable for this scope. However, simply using the time averaged coordinates still proved not sufficient for a coherent definition of the quantum zone, as the dimers themselves can 'move' from linking a pair of atoms to another pair along the same dislocation line, or to a pair belonging to the next migration site on the glide plane. A very simple hysteretic algorithm was thus used, in which the quantum zone was updated only if the number of QM core atoms calculated at a given time along the system trajectory was greater than that in the 'perfect' core determined at the beginning of the simulation, i.e. if a new dimer pair had formed in the neighbouring Peierls valley.

Figure 5 shows a histogram of the time elapsed between the beginning and the end of a core migration event into the next Peierls valley. This is the time taken for a migration once the initial kink has formed. The longest migration step takes around 5 ps to complete, whereas seven of the observed steps occur just within 2 ps. These results suggests two different migration modalities, one associated with a typical time centred around 2000 fs and a second, less frequent one, taking around 4500 fs to complete. Direct analysis of the motion patterns associated with the events occurring at these two timescales allows to establish that two different mechanisms are indeed operating. This is illustrated in figures 6 and 7.

Figure 6 portraits the migration event occurring via the 'slower' mechanism. Each sub-figure is labelled by its corresponding simulation time along the system trajectory, panel (a) showing the core configuration at $t = 42.8$ ps, and

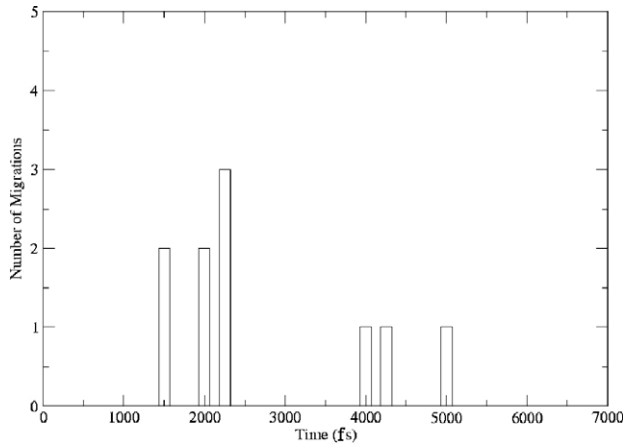

Figure 5. Histogram demonstrating the length of time taken for each migration step, from a perfect core position to the next core position in the lattice. The time interval width is set to 50 fs.

the final panel (h), corresponding to $t = 48.5$ ps. The first panel (a) shows the core structure before it begins to migrate. One important thing to note is the prevalence of solitons along the dislocation core line. At this temperature and strain, only two complete dimer pairs are visible, the rest of the atoms being unbound. Panel (c) reveals the formation of a double kink, developed from the anti-phase defect (APD) originally lying between the two dimers in panel (a). This suggests that the presence of anti-phase defects directly influences kink formation, although this effect was not investigated in previous analyses [8, 12] for simplicity. The next step in the migration is shown in panel (e), and consists of the formation of a square complex at the dislocation line (bottom of the panel). Once more, the precursor of the structure observed is an APD lying immediately beneath the dimer. The square complex then forms a new bond with an atom in the dimer pair (panels (f), (g)) and the original dislocation line eventually migrates to the neighbouring Peierls valley (panel (h)), with the majority of the dislocation core again consisting of APDs rather than stable dimerized pairs as in the beginning of the process.

Figure 7 illustrates one of the 'quicker' migration steps discussed above. As before, the initial core configuration contains many APDs as well as dimers, and, crucially, in panel (c) a square complex has formed on the dislocation line, seeded by an APD, with two dimers remaining above and below it. The square complex then proceeds to migrate along the core and in a 'zipper'-like motion (upwards in the snapshot sequence shown), forming regular hexagonal rings on its left and creating APDs and new dimers in the neighbouring Peierls valley as it does so. Panels (f) and (g) are reminiscent of the migration observed in figure 6. The quick migration mode relies on the formation of a square complex, as seen in slide (c), which is seeded by an APD, followed by the subsequent migration, rather than break-up, of that complex along the dislocation line. This is achieved by a concerted bond switching mechanism that effectively shifts dimer pairing to the next neighbouring Peierls valley along the partial motion direction.

To summarize, in this short four-dimer dislocation line segment, simulated at 600 K under 5% strain we are able to observe different types of motion corresponding to different typical migration times. APDs are ubiquitous in our simulations in these conditions, suggesting their relevance for the microscopic mechanism of migration of the present Si dislocation system and quite possibly other high Peierls barrier materials.

4. Conclusion

Using the LOTF hybrid scheme we have been able to model the migration of the dissociated screw dislocation in silicon

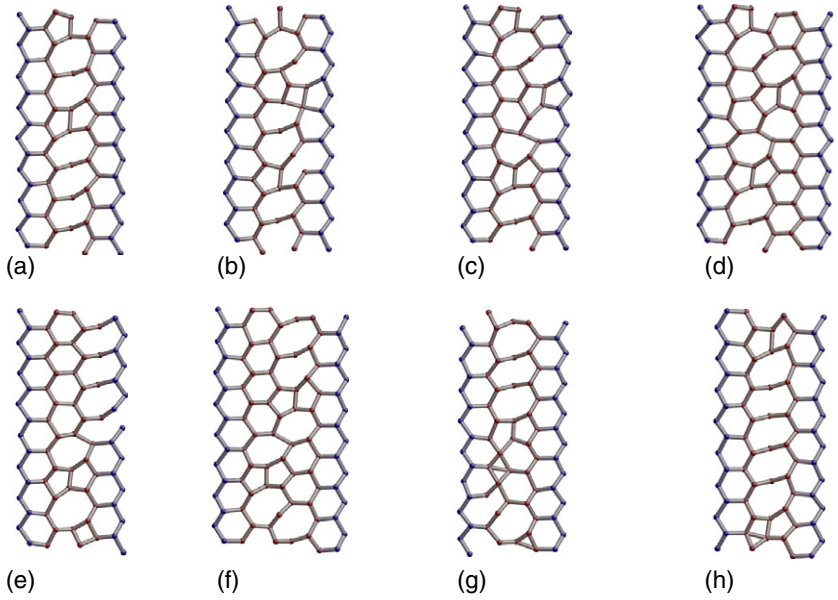

Figure 6. Slow migration step; a double kink is initially formed, eventually leading to kink migration along the remainder of the dislocation line. (a) 42.82 ps; (b) 43.70 ps; (c) 44.16 ps; (d) 44.40 ps; (e) 45.42 ps; (f) 46.04 ps; (g) 47.78 ps; (h) 48.52 ps.

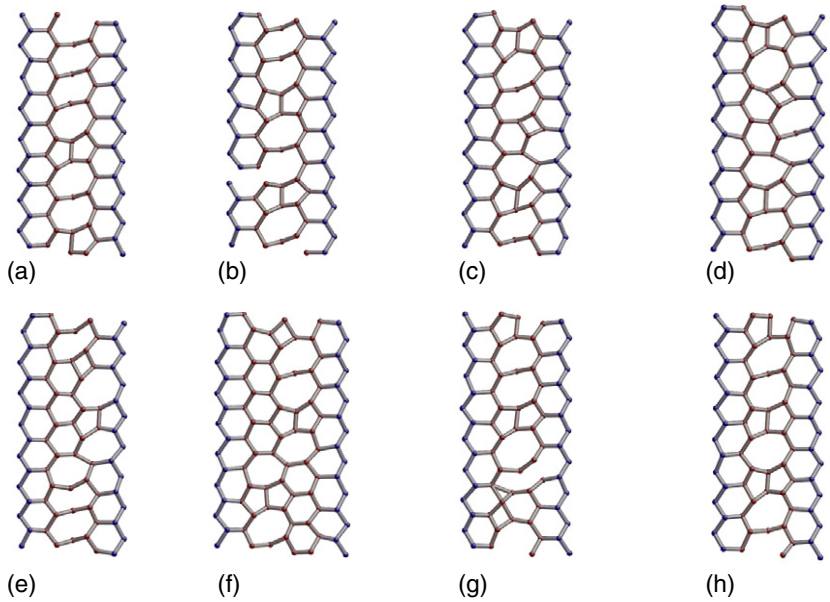

Figure 7. Quicker migration step; the square complex formed in (c) migrates the length of the dislocation line, 'pulling' trailing dimers across to the next Peierls valley in a zipper-like upwards motion. (a) 81.40 ps; (b) 81.48 ps; (c) 82.34 ps; (d) 82.58 ps; (e) 82.92 ps; (f) 83.36 ps; (g) 84.38 ps; (h) 84.82 ps.

over a 100 ps time scale, and to observe the bond switching paths involved in kink formation and migration. In the classical picture [1], the role of undimerized core Si atoms (such as those associated with APDs) in kink formation and migration is not prominent, while our simulations suggest that any complete analysis of kink formation rates should take their structures into account. Indeed, while several authors [12, 17] have studied the characteristics of APDs in the 30° partial in a static context, our observation of the prevalence of such defects under conditions of high strain suggest them as the likely precursors to double kink formation, which is the dislocation migration limiting step. We find that the Stillinger–Weber potential is not sufficiently accurate to investigate the delicate bond breaking/forming processes occurring along dislocation migration, at most providing useful order of magnitude insights into the relevant strain fields and simulation timescales required to study the migration. However, the silicon bulk region modelled by the Stillinger–Weber classical potential is an effective medium for the transmission of the applied stress field to the dislocation cores, provided that its use is limited to four-fold coordination regions and moderate strain values, and that the correct elastic boundary conditions are supplied by using a QM model to determine the relaxed core region structure.

The QM region must extend well beyond the dimerized atoms on the dislocation line, revealing that an explicit electronic structure representation must be used to model the first and second nearest neighbours of the core atoms in order to observe core migration. Our results further suggest that kink formation readily occurs in spite of the energy gain associated with dimer bonding along the core. Indeed, in all the migration events observed in our simulations many of the core atoms are undimerized for a large fraction of time, so that the energy involved in breaking the dimer bond does not appear to be a limiting factor for migration. In particular, two distinct migration pathways emerged, one involving conventional double kink formation and subsequent migration (figure 6) and a second, quicker one involving coherent motion of a square complex along the dislocation line (figure 7). Although our simulations were performed using high driving stresses and a small periodically repeated core length involving eight core atoms only, the observed behaviour is rich in character. Nonetheless we note that simulations using longer dislocation cores may add on the present results by revealing further dislocation migration mechanisms. Future work on this problem will further explore the effects of varying the dislocation core lengths and simulation temperature on the predicted migration pathways. Once the main migration steps are determined, the hybrid scheme used in this work could be redirected to calculating their associated free energy barriers, to improve on the poor statistics obtained by the simple MD simulation approach. This could be achieved e.g., by carrying out thermodynamic integrations based on the accurate forces available in the QM regions.

Acknowledgments

ADV acknowledges support from the EPSRC Grant EP/C5239 38/1, the EU-FP7-NMP Grant 'ADGLASS', and Rio Tinto Technological Resources Pty Limited. CG acknowledges technical help and discussions with James Kermode. ADV gratefully acknowledges Michael John Gillan for over two decades of illuminating discussions, encouragement and advice.

References

[1] Hirth J P and Lothe J 1982 *Theory of Dislocations* (Malabar, FL: Krieger)
[2] Ray I L F and Cockayne D J H 1971 *Proc. R. Soc.* A **325** 534
[3] Gomez A, Cockayne D J H, Hirsch P B and Vitek V 1975 *Phil. Mag.* **31** 105
[4] Gomez A and Hirsch P B 1978 *Phil. Mag.* A **38** 733
[5] Marklund S 1978 *Phys. Status Solidi* b **85** 673
[6] Hirsch P B 1979 *J. Physique* **40** C6–40
[7] Oberg S, Sitch P K, Jones R and Heggie M I 1995 *Phys. Rev.* B **51** 13138
[8] Oyama N and Ohno T 2004 Migration processes of the 30° in silicon *Phys. Rev. Lett.* **93** 195502
[9] Pizzagalli L, Pedersen A, Arnaldsson A, Jonsson H and Beauchamp P 2008 Theoretical study of kinks on screw dislocation in silicon *Phys. Rev.* B **77** 064106
[10] Lehto N and Oberg S 1998 Effects of dislocation interactions: application to the period-doubled core of the 90° partial in silicon *Phys. Rev. Lett.* **80** :5568
[11] Hansen L B, Stokbro K, Lundqvist B I and Jacobsen K W 1996 Dynamics of partial dislocations in silicon *Mater. Sci. Eng.* B **37** 185–8
[12] Nunes R W, Bennetto J and Vanderbilt D 1998 Atomic structure of dislocation kinks in silicon *Phys. Rev.* B **57** 10388
[13] Bulatov V V, Yip S and Argon A S 1995 Atomic modes of dislocation mobility in silicon *Phil. Mag.* A **72** 453–96
[14] Scarle S, Ewels C P, Heggie M I and Martsinovich N 2004 Linewise kinetic Monte Carlo study of silicon dislocation dynamics *Phys. Rev.* B **69** 075209
[15] Cai W, Bulatov V V, Justo J F, Argon Ali S and Yip S 2000 Intrinsic mobility of a dissociated dislocation in silicon *Phys. Rev. Lett.* **84** 3346–9
[16] Jones R 2000 *Mater. Sci. Eng.* B **71** 24–9
[17] Csanyi G, Engeness T D, Ismail-Beigi S and Arias T A 2000 *J. Phys.: Condens. Matter* **12** 10029–37
[18] Bulatov V 2001 *Scr. Mater.* **45** 1247–52
[19] Csányi G, Albaret T, Payne M C and De Vita A 2004 Learn on the fly: a hybrid classical and quantum-mechanical molecular dynamics simulation *Phys. Rev. Lett.* **93** 175503
[20] Kermode J R, Albaret T, Sherman D, Bernstein N, Payne M C, Csányi G and de Vita A 2008 Low speed fracture instabilities in a brittle crystal *Nature* **455** 1224–7
[21] Moras G, Colombi Ciacchi L, Csányi G and de Vita A 2007 Modelling (100) hydrogen induced platelets in silicon with a multi-scale molecular dynamics approach *Physica* B **401/402** 16–20
[22] Stillinger F H and Weber T A 1985 Computer simulation of local order in condensed phases of silicon *Phys. Rev.* B **31** 5262
[23] Kwon I, Biswas R, Wang C Z, Ho K M and Soukoulis C M 1994 Transferable tight-binding models for silicon *Phys. Rev.* B **49** 7242
[24] Sherman D and Beery I 2004 Dislocation deflect and perturb dynamically propagating cracks *Phys. Rev. Lett.* **93** 265501
[25] Gattinoni C *et al* 2010 in preparation
[26] Csanyi G, Albaret T, Moras G, Payne M C and De Vita A 2005 *J. Phys.: Condens. Matter* **17** 691–703
[27] Bernstein N, Kermode J R and Csányi G 2009 *Rep. Prog. Phys.* **72** 026501